Journal of
Ceramic Science
and Technology

Effects of Aging Time on Microstructure, Hydrophobic and Optical Properties of BiFeO$_3$ Thin Films Synthesized via Sol-Gel Method

H. Baqiah[1], Z.A. Talib[*1], A.H. Shaari[1],
M. M. Awang Kechik[1], J.Y.C. Liew[1], N.B. Ibrahim[2]

[1]Physics Department, Faculty of Science, Universiti Putra
Malaysia, 43400 UPM, Serdang, Selangor, Malaysia
[2]School of Applied Physics, Faculty of Science and Technology, Universiti
Kebangsaan Malaysia, 43600 Bangi, Selangor, Malaysia

Abstract

BiFeO$_3$ (BFO) films were synthesized with the sol-gel method followed by the spin coating technique using 2-methoxyethanol as solvent and acetylacetone as chelating agent. The effects of aging time (t = 0, 1, 3, 6 days) of the BFO sol on the microstructure, wettability and optical properties of BFO films were investigated by means of X-ray diffraction (XRD), atomic force microscopy (AFM), contact angle (*CA*) measurement, Uv-vis and photoluminescence. The crystallinity of films was affected by t. Crystallite size of the films changed slightly in the range of 14.2 – 15.2 nm while the lattice parameters clearly varied with t. The average particle size of BFO films ranged between 45.9 and 52.7 nm while the mean square roughness (R_q) varied between 1.0 and 4.2 nm. The films showed maximum optical transmittance (81 – 90 %) in the range 600 – 800 nm. The band gap of the films was also affected with t, and it has a value of 2.85 to 2.76 eV. The films showed a hydrophobic property with *CA* ranging between 95.3 to 104.7 °. The best crystallinity, lowest R_q and highest E_g = 2.85 eV were obtained for the film with t = 1 day. The results demonstrate possible development of a superhydrophobic coating using BiFeO$_3$ coating.

Keywords: BiFeO$_3$ films, wettability, aging time, roughness, band gap

I. Introduction

BiFeO$_3$ (BFO) ceramic has received significant attention among multiferroic materials because it is the only single-phase material that combines antiferromagnetic and ferroelectric properties at ambient temperature [1]. This has made it a material suitable for next-generation spintronic applications [2]. For example, BiFeO$_3$ thin film can be used to fabricate effective resistive random access memory devices [3]. In addition, BFO shows a relatively small band gap (E_g) ranging from 2 – 3 eV, which makes it useful for various applications [4]. For example, extensive research has been undertaken to manipulate its ferroelectric and optical properties for use in photocatalytic applications [5]. Some studies have focused on the engineering of E_g for the improvement of photovoltaic efficiency as well as of photocatalytic performance [5–7].

The search for hydrophobic ceramic has been a subject for many researchers as it can be used in a broad range of applications [8–11]. Some ceramics such as rare earth oxides are intrinsically hydrophobic owing to their electronic structure which hinders the bonding of hydrogen water molecules with their surface [12]. Other oxides, such as Fe$_3$O$_4$ and gamma-Fe$_2$O$_3$ [13], have exhibited hydrophobicity in nanoscale form while high rough morphology feature can enhance surface hydrophobicity as found in the hierarchical microstructure of Bi/Bi$_2$O$_3$ [14]. Until now, there have been few studies concerning the understanding of interface of water with BFO. Hence, many researchers have shown justifiable interest in evaluating the wettability of BFO nano-crystalline film.

BFO ceramic has been extensively investigated in bulk, thin film and nanostructure form [2]. BFO thin film has a rich physico/chemical phenomenon because its structure, ferroelectric, magnetic and optical properties can be tuned according to its substrate and growth condition [15]. Hence, several fabrication methods such as pulsed laser ablation, RF sputtering, hydrothermal and sol-gel methods have been employed to synthesize BFO thin film [2, 15]. Among these methods, the sol-gel method has many advantages, such as low cost and relatively simple experimental setup, and can be used to obtain high-quality films [3, 16, 17]. From previous research, the synthesis of BFO with the sol-gel method often involves the addition of more than one agent such as acetic acid, ethylene glycol, ethanol amine, etc. to obtain the sol [18–20]. Beside the chelating agent, the sol-gel method entails parameters such as solution concentration [21], sintering temeperature [22], aging time [23]. The aging time of the sol is one of the factors that affects the final properties of the film. For example, the physical properties of ZnO thin film were dependent on the sol aging

* Corresponding author: zainalat@upm.edu.my

time, the best crystallity, roughness, photoluminescence being observed for film synthesized using sol aged for 11 days [23]. For BFO, there are scarcely any studies about the effect of aging on the microstructure of films synthesized from this. To obtain BFO film with good quality, it is important to optimize the sol aging time. Hence, in this research, we aimed to investigate the microstructure, wettability and optical properties of BFO synthesized with the sol-gel method followed by spin coating from sol aged for 0, 1, 3 and 6 days using acetylacetone as the chelating agent.

II. Experimental Details

The sol-gel method followed by the spin coating technique was used to prepare $BiFeO_3$ thin films on glass substrate. Bismuth nitrate pentahydrate, $Bi(NO_3)_3 \cdot 5H_2O$, and iron nitrate nonahydrate, $Fe(NO_3)_3 \cdot 9H_2O$, were used as raw materials while 2-methoxyethanol (2MOE) and acetylacetone (AcAc) were used as a solvent and chelating agent, respectively. First, $Bi(NO_3)_3 \cdot 5H_2O$ and $Fe(NO_3)_3 \cdot 9H_2O$, with 1:1 molar ratio, were separately dissolved in 2MOE and magnetically stirred for 1 h. A few drops of AcAc were added during the stirring of iron nitrate solution, with AcAc to Fe^{3+} molar ratio of 3:1. The $Bi(NO_3)_3 \cdot 5H_2O$ and $Fe(NO_3)_3 \cdot 9H_2O$ solutions were mixed together and magnetically stirred for 2 h. The pH of the final solution is about 0.33. The obtained sol was filtered using a 0.45-μm syringe and aged for 0, 1, 3, 6 days. A few drops of the aged sol were then deposited on a cleaned glass substrate (2 x 2.4 cm) and spin-coated at 1500 rpm for 30 s. The films were then dried at 120 °C for 10 min and then at 380 °C for 5 min. The deposition process was repeated to form a second BFO layer. Finally, the dried films were sintered at 550 °C for 1 h. The films obtained with this procedure for sol aged at time ($t = 0, 1, 3, 6$ days) were labelled as 0 d, 1 d, 3 d and 6 d films.

The film structure was characterized with the X-ray diffraction technique (XRD, Panalytical X'pert Pro DY 1861) with CuKα radiation source ($\lambda = 1.5418$ Å) and the microstructure of films was studied using atomic force microscopy (AFM, Bruker, model dimension edge). The water wettability of the films was evaluated using contact angle (CA) measurement (CA, Thetalite 100). The optical properties were studied using an UV-vis spectrophotometer (UV-vis, Perkin Elmer (Lamda35)) and a photoluminescence spectrofluorometer (PL, Perkin Elmer LS-55).

III. Results and Discussion

(1) Crystal structure anlaysis

Fig. 1 shows the XRD patterns of $BiFeO_3$ films. All the films were in a single phase that matched well with the rhombohedral structure of $BiFeO_3$ (ICSD No 01−071−2494), except for the 6 d film where traces of phase related to Bi_2O_3 and $Fe_{0.942}O$ were identified. Amorphous-like phase is observed in the 0 d $BiFeO_3$ film. The film deposited from sol aged at $t > 0$ day showed better crystallinity while the best crystallization was observed in the 1 d film. This demonstrates that the aging time is a crucial factor affecting the crystallization process of film. During the aging process, there is a possible reaction between metal nitrate and acetylacetone, and that results in the formation of metals complex [24]. The aging time may play a role in the accomplishment of this reaction and form a stable solution. This means that stable solution formed after one-day aging time while it degraded after six days of aging and decomposed to Bi_2O_3 and FeO phases.

The crystallite size of the films was calculated using the Scherrer equation given by

$$d = \frac{0.9\lambda}{\beta \cos\theta} \qquad (1)$$

where λ, β and θ are X-ray wavelength, half width at half maximum and Bragg angle of diffraction peaks, respectively. The crystallite size of films ranged between 14.3 and 15.2 nm. The lattice parameters a and c of the films were calculated by means of Rietveld analysis using High-Score Plus software and listed in Table 1. Fig. 1c shows the Rietveld analysis of the 1 d film together with simulated unit cell drawn using Vesta software. The goodness of fit is listed in Table 1. There was a clear variation of lattice parameters for the films. This resulted in lattice strain, which could be due to the presence of amorphous-like phase or the growth of $BiFeO_3$ on glass substrate followed by shrinkage after the annealing process. The lattice strain was evaluated based on comparison with lattice parameters, a' and c' of the standard (ICSD No 01−071−2494) using the following equations [21],

$$\Delta\varepsilon_a = \frac{a - a'}{a'} \qquad (2)$$

$$\Delta\varepsilon_c = \frac{c - c'}{c'} \qquad (3)$$

Table 1: Lattice parameters, a and, c, lattice strains, $\Delta\varepsilon_a$ and $\Delta\varepsilon_c$, crystallite size, roughness (Rq), contact angle (CA), particles size, band gap, E_g and goodness of fit (GOF) of $BiFeO_3$ films.

Aging time (t) (days)	a (Å)	c (Å)	$\Delta\varepsilon_a$ × 10⁻³	$\Delta\varepsilon_c$ × 10⁻³	Crystallite size (nm) from XRD	R_q (nm)	CA (°)	Particle size (nm) from AFM	E_g (eV)	GOF
0	5.569(3)	13.86(1)	-3.3±0.5	-0.5±0.7	14.6±0.70	2.1	97.2±0.3	46.9±19.4	2.78±0.05	1.0
1	5.5742(5)	13.803(2)	-2.4±0.1	-4.6±0.1	14.3±0.25	1.0	104.5±0.4	45.9±21.2	2.85±0.07	3.1
3	5.564(1)	13.827(3)	-4.2±0.2	-2.9±0.2	15.2±0.04	4.2	104.7±0.5	52.7±27.3	2.76±0.05	1.1
6	5.568(1)	13.805(7)	-3.5±0.2	-4.5±0.5	14.6±0.21	3.7	95.3±0.5	mix of 14−20 nm and ~ 77 nm	2.79±0.03	1.0
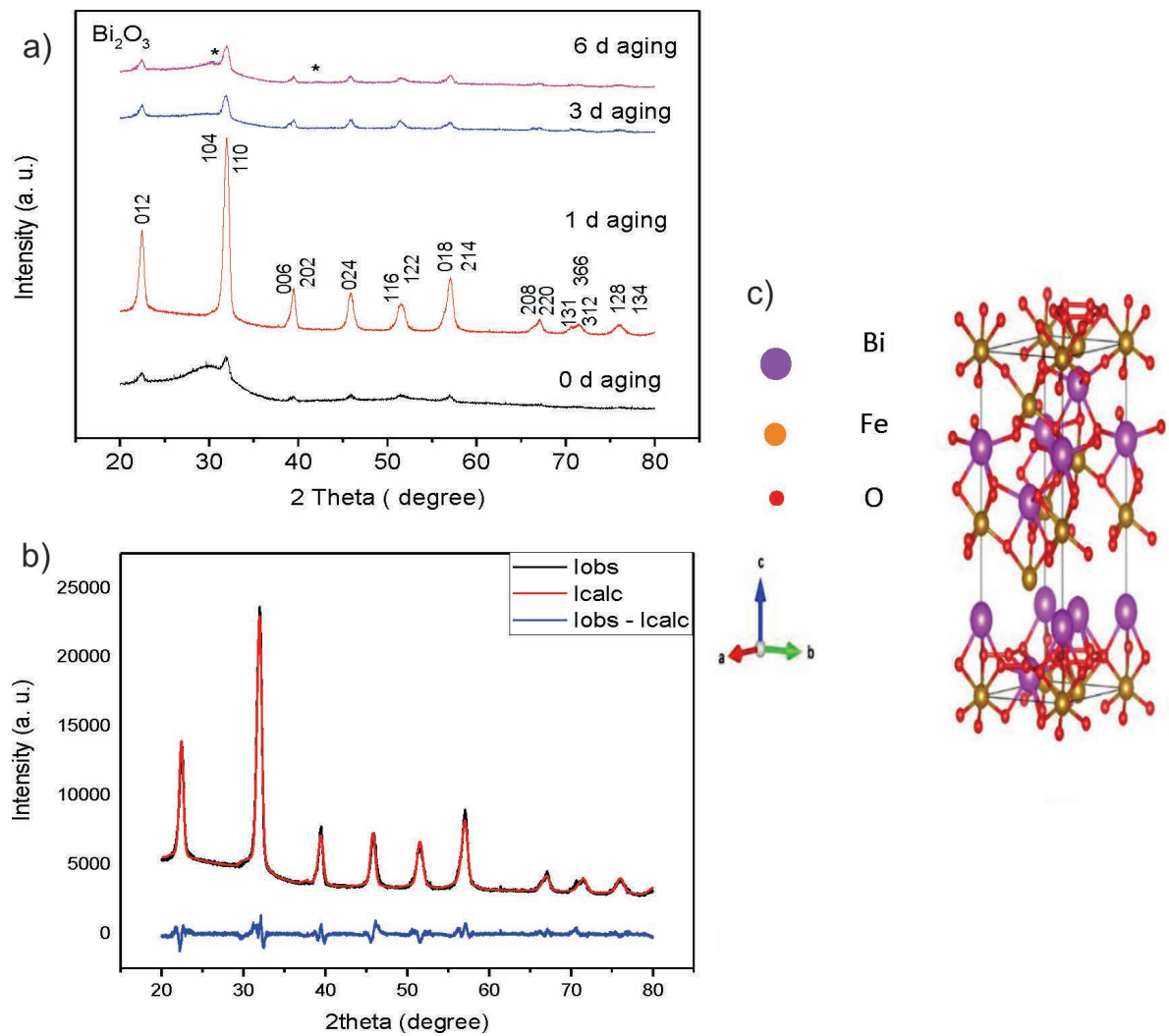
Fig. 1: a) XRD of BiFeO$_3$ thin films deposited from sol aged at 0, 1, 3 and 6 days, b) Rietveld analysis of 1 d film and c) simulated unit cell of 1 d film.

From the lattice strains listed in Table 1, it can be deduced that the films have a compressive strain and, overall, there is no systematic change of the lattice strain with aging time. The maximum $\Delta\varepsilon_c = -4.6 \times 10^{-3}$ and minimum $\Delta\varepsilon_a = -2.4 \times 10^{-3}$ were observed in the 1 d film, however, this trend was inversely changed in the case of the 3 d film.

(2) Microstructure analysis

Fig. 2 presents 2-dimensional (2D) and 3-dimensional (3D) AFM micrographs of BiFeO$_3$ films. The AFM images corroborate well with the XRD result. Some regions of the 0 d micrograph shows a well-defined polycrystalline structure that may refer to crystalline BiFeO$_3$. Polycrystalline morphology becomes more obvious in films with d > 0. Fine particles together with big particles that may be referred to Bi$_2$O$_3$ or Fe$_{0.92}$O are observed in the 6 d films. The root mean square roughness, R_q, of films was calculated using Nanoscope analysis software. The smallest R_q, indicating a smooth surface, was found in the 1 d BiFeO$_3$ film. The R_q decreased from 2.1 nm for the 0 d film to 1 nm for the 1 d film and then increased to 4.2 nm for the 3 d film. The particle size of the films was analysed in the 2D images using the above-mentioned software. The average particle size of the films is listed in Table 1. The average particle size

of the films ranged between 46.9 and 52.7 nm for the 0 d and 3 d films, respectively. The 6 d film has a mix of big particles, ~ 77 nm, which may be related to secondary phases observed in the XRD result and the small particles with sizes between 14 ~ 20 nm which may be related to BiFeO$_3$ phase.

(3) Hydrophobic property

The contact angle (*CA*) was measured to assess the surface wettability of BiFeO$_3$ films, which is an essential property for many applications [12]. Fig. 3 shows the water *CA* of BiFeO$_3$ films. The *CA* of the films ranged from 95.3 to 104.7 °, which means that the BiFeO$_3$ nano-crystalline film surface is hydrophobic. The *CA* increased from 97.2 to 104 ° while the R_q decreased from 2.1 to 1 nm for the 0 d and 1 d films, respectively, which suggests that the hydrophobic property was enhanced with the improvement in BFO crystallinity. On the other hand, the *CA* was maintained at 104.7 ° for the 3 d film although it has lower crystallinity than the 1 d film, which could be due to the increase in surface roughness. The lowest *CA* was found in the 6 d film, which has some secondary phase and inhomogeneous surface morphology. Hence, the *CA* of the films may be affected by the crystallinity and roughness as well as the presence of secondary phases in the films.
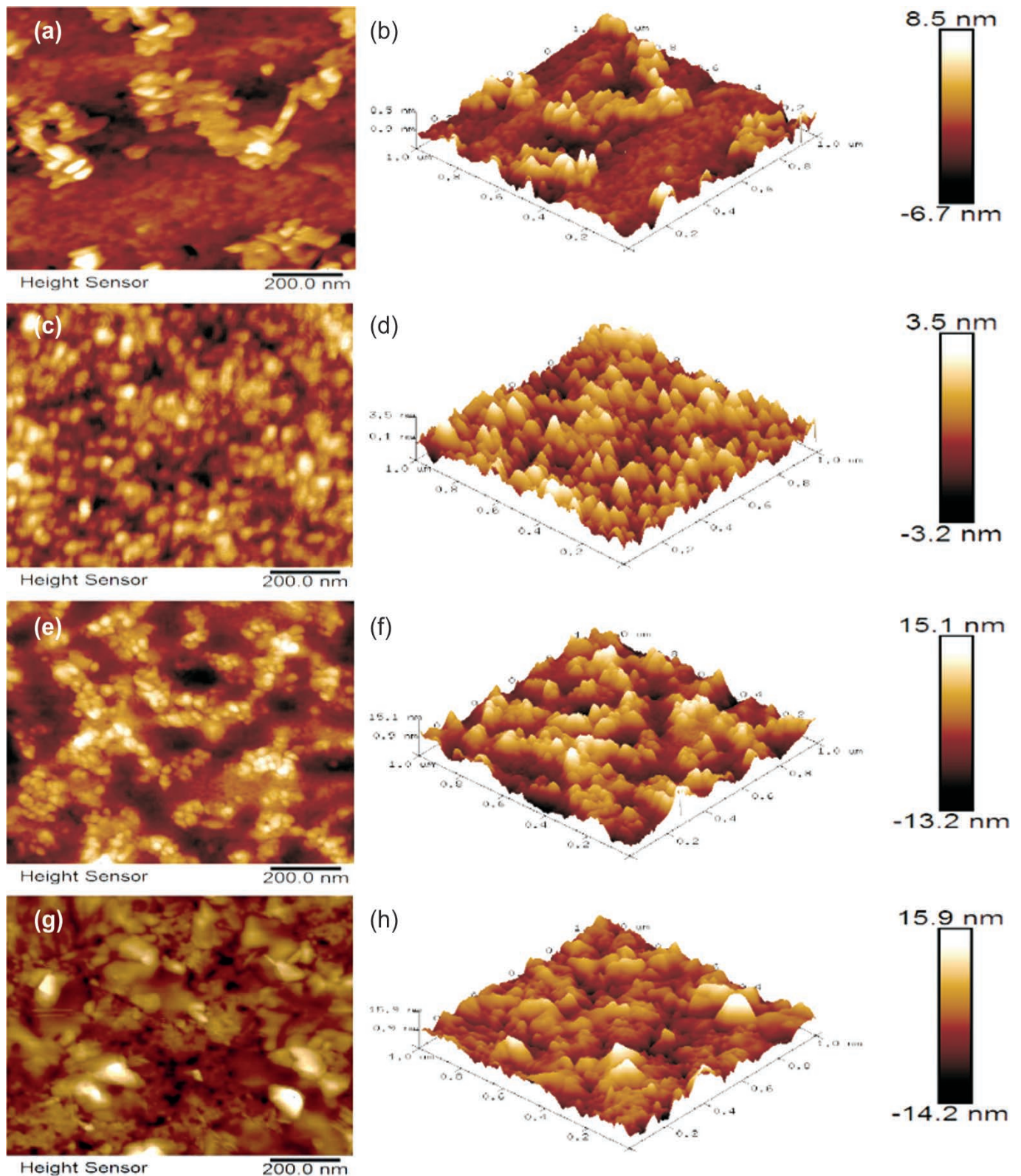
Fig. 2: AFM micrographs of BiFeO$_3$ thin films, (a-b) 0 d aging, (c-d) 1 d aging, (e-f) 3 d aging, and (g-h) 6 d aging.

(4) Optical transmittance and band gap evaluation

The optical transmittance of the films was evaluated using an UV-vis spectrophotometer in the wavelength of 300–800 nm as shown in Fig. 4. It is shown that film without aging has clearly shifted to high wavelength above 470 nm and shows the highest transmittance ~ 95 % at ~ 700 nm wavelength. The transmittance of films prepared from aged sol reached its maximum value at around 600 nm wavelength and then slightly decreased. Maximum absorption of films occurred at wavelength less than 600 nm. The average transmittance in the range of 600 – 800 nm is 90, 85, 87 and 81 % for films with 0 d, 1 d, 3 d and 6 d, respectively. To evaluate the band gap E_g of BiFeO$_3$ thin films, the Kubelka-Munk function, $F(R)$, was calculated from
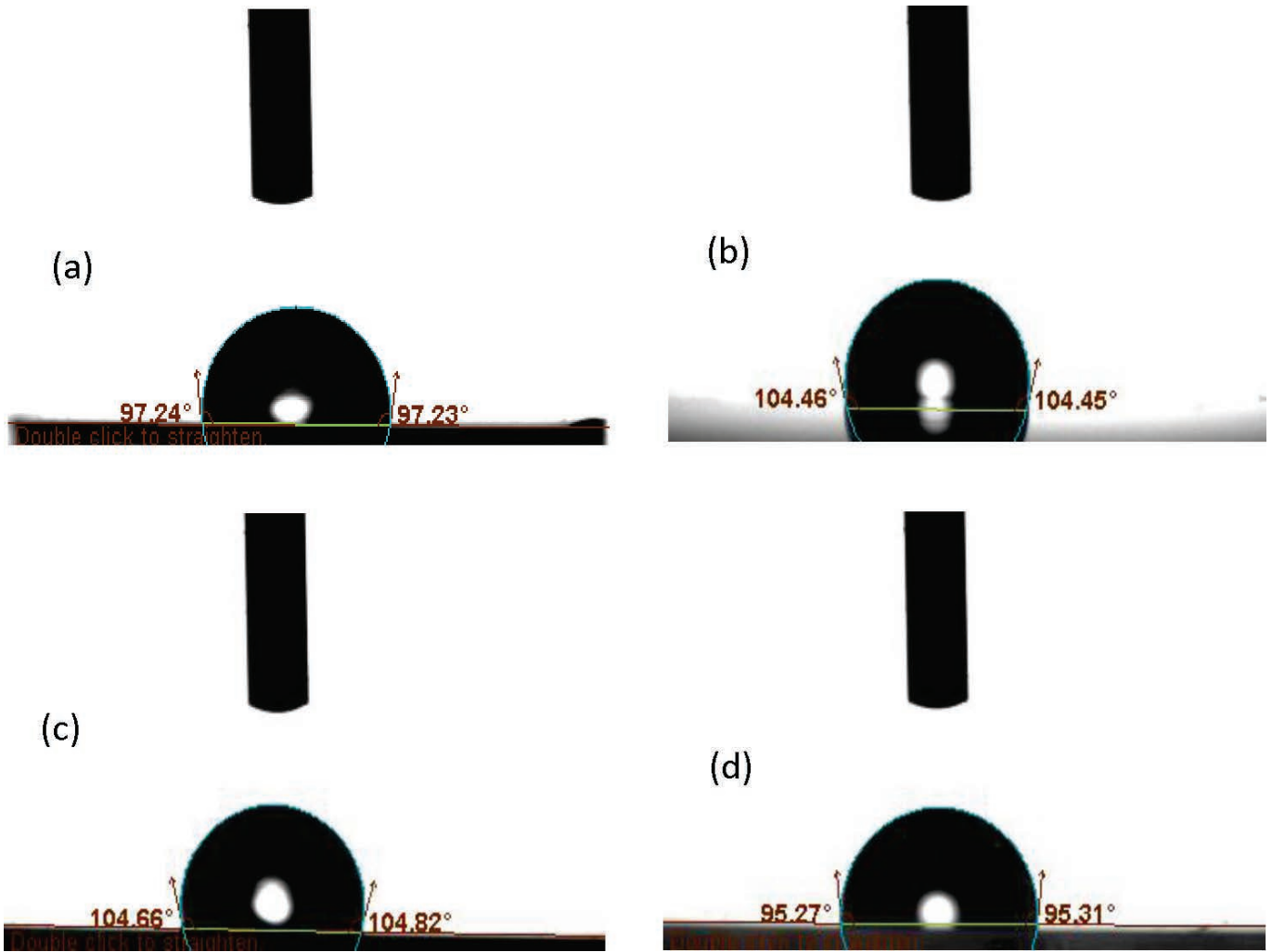
Fig. 3: Contact angles of water on BiFeO$_3$ surface thin films, (a) 0 d aging, (b) 1 d aging, (c) 3 d aging, and (d) 6 d aging.

diffuse reflectance spectra using [25], $F(R) = \frac{(1-R)^2}{2R}$. Here, the direct band gap was determined by extrapolating a straight line from the $(F(R)\,h\nu)^2$ vs. $h\nu$ plot to the corresponding E_g value at $h\nu = 0$, as shown in Fig. 5. The E_g of the films is listed in Table 1. The E_g varied from 2.76 eV for the 3 d BiFeO$_3$ film to 2.85 eV for the 1 d film. These values are in good agreement with those reported in the literature for the band gap of BiFeO$_3$ thin film [26, 27]. There is no trend between E_g and BiFeO$_3$ films and the aging time of the sol used. Several factors that affect the E_g values of BiFeO$_3$ films have been reported. Chen *et al.* account for the decrease in E_g from 2.75 to 2.71 eV for thin film annealed at 500 and 600 °C, respectively, based on grain enlargement and reduction of amorphous phases for the film annealed at the higher temperature [27]. Another report indicates that the E_g was affected by the film compressive strain [28]. Liu *et al.* showed that compressively strained BiFeO$_3$ has a large band gap of 3.12 eV while it has smaller E_g, of 2.75 eV when it has tensile strain [29]. This means that a change in the lattice parameters or lattice strain will affect the E_g value [4]. To identify the relation between lattice strain and E_g of BiFeO$_3$ thin film in this work, the E_g, $\Delta\varepsilon_a$ and $\Delta\varepsilon_c$ were plotted against the aging time, *t*, as shown in Fig. 4b. It can be easily noticed that there is a proportional trend between the E_g and $\Delta\varepsilon_c$, while a reverse trend between the E_g and
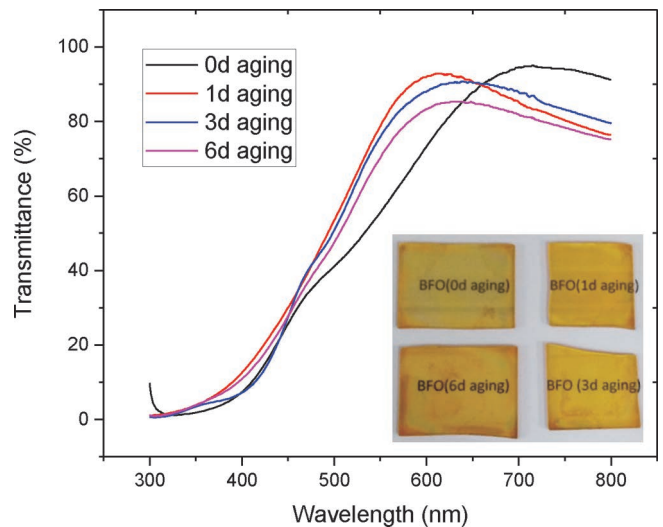
Fig. 4: Optical transmittance of BiFeO$_3$ films.

$\Delta\varepsilon_a$ emerged. The dependence of E_g with $\Delta\varepsilon_c$ is in good agreement with previous report, where the largest E_g was observed for highly compressively strained BiFeO$_3$ thin film and it became smaller as compressive strain was relieved [21, 29].
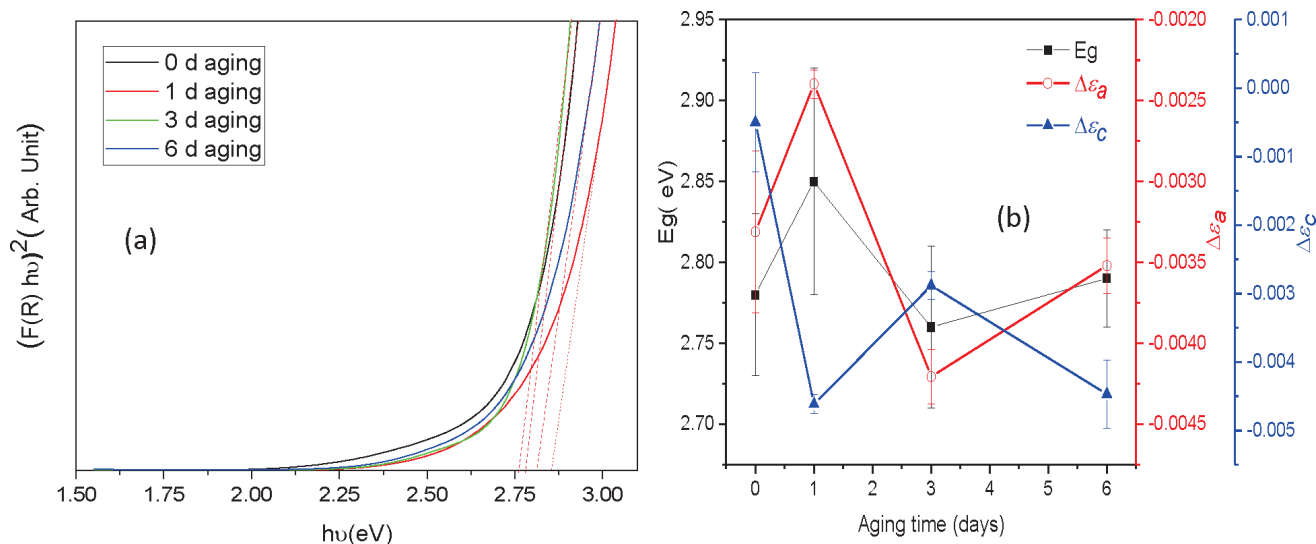
Fig. 5: a) $(F(R) h\nu)^2$ vs $h\nu$ of BiFeO$_3$ thin films. b) Correlations between $\Delta\varepsilon_a$, $\Delta\varepsilon_c$ and E_g with aging time for BiFeO$_3$ thin films.

(5) Photoluminescence properties

Fig. 6 shows PL spectra of BiFeO$_3$ films using excitation wavelength, $\lambda = 400$ nm. Three emission peaks can be obtained via fitting with Gaussian function as indicated in the inset of Fig. 6. These peaks are centered at 459.6, 533.5 and 586.7 nm for the 0 d film. The first peak observed at 459.6 nm, can be assigned to near-band-edge emission (NBE) resulting with electron transition from conduction band to the valence band of BiFeO$_3$. This peak is located at 446.1, 465.2 and 457.3 nm for the 1 d, 3 d and 6 d films. The variation of NBE peak positions corroborated well with the changed of E_g measured from the reflectance measurement. Moreover, intensity of this peak varied with changing aging time, indicating a different rate of electron-hole recombination for the films. The highest intensity was observed for the 1 d film while the lowest intensity was found for the 0 d film. The second peak observed at 533.5 nm is related to defect-like oxygen vacancy that is abundant in the BiFeO$_3$ system [30, 31]. This peak was found to be sharp and intense for the 3 d film, indicating a high amount of oxygen vacancies. The third peak located at 586.7 nm is associated with d-d transition in energy levels of Fe ions in BiFeO$_3$ [32].
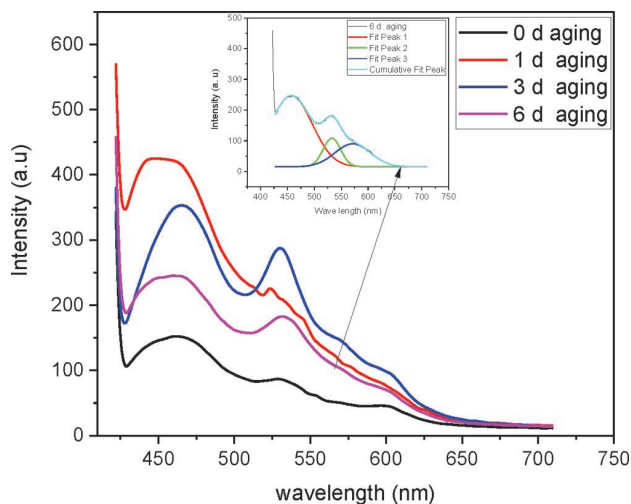
IV. Conclusions

BiFeO$_3$ films were successfully synthesized with the sol-gel method using acetylacetone as a chelating agent. The aging time is a crucial factor that affects the crystallinity, phase formation, hydrophobicity and optical properties of the films. The films were grown in single phase of BiFeO$_3$ except the 0 d film that involved amorphous-like phase and the 6 d film which contained traces of Bi$_2$O$_3$ and Fe$_{0.92}$O. The crystallite size of the films varies between 14.3 and 15.6 nm while the lattice parameters of BFO films has a strong dependence on t. The highest strain of lattice parameter c, $\Delta\varepsilon_c = 4.6 \times 10^{-3}$ was observed in the 1 d film while the lowest $\Delta\varepsilon_c = 0.7$ was found in the 0 d film. The R_q and average particle size increased from 45.9 and 1.0 nm, respectively for the 1 d film to 52.7 and 4.2 nm respectively for the 3 d film. Contact angle measurement found that the film is hydrophobic with CA values between 95.3 and 104.7 °. The results suggest that the enhancement of hydrophobicity in the 1 d and 3 d films relates to the film crystallinity and roughness. The films show maximum transmittance (81 – 90 %) at 600 – 800 nm wavelength. The E_g value varied in the range of 2.76 – 2.85 eV. Based on comparison of the E_g value and lattice strain ($\Delta\varepsilon_c$), it was found that there is a proportional trend between the E_g and the $\Delta\varepsilon_c$. The PL spectra of films contain three peaks corresponding to NBE, oxygen defect and d-d transition in energy levels of Fe ions in BFO. The intensity of NBE peaks was varied for the films, the lowest and highest intensity being found for the 0 d and 1 d films, respectively. The results suggest that 1 day is the optimum aging time for obtaining single-phase BFO film with good crystallinity, hydrophobicity and roughness.

Acknowledgement

Fig. 6: PL spectra of BiFeO$_3$ thin films excited at wavelength of 400 nm. Inset fitted curve of Pl spectra of 6 d aging film.

References

1   Catalan, G., Scott, J.F.: Physics and applications of bismuth ferrite, *Adv. Mater.*, **21**, 2463 – 2485, (2009).

2   Wu, J., Fan, Z., Xiao, D., Zhu, J., Wang, J.: Multiferroic bismuth ferrite-based materials for multifunctional applications: ceramic bulks, thin films and nanostructures, *Prog. Mater. Sci.*, **84**, 335 – 402, (2016).

3   Kumari, C., Varun, I., Tiwari, S.P., Dixit, A.:. Robust nonvolatile bipolar resistive switching in sol-gel derived BiFeO₃ thin films, *Superlattices Microstruct.*, **120**, 67 – 74, (2018).

4   Satar, N.S.A., Aziz, A.W., Yaakob, M.K., Yahya, M.Z.A., Hassan, O.H., Kudin, T.I.T., Kaus, N.H.M.: Experimental and first-principles investigations of lattice strain effect on electronic and optical properties of biotemplated BiFeO₃ nanoparticles, *J. Phys. Chem. C.*, **120**, 26012 – 26020, (2016).

5   Bai, X., Wei, J., Tian, B., Liu, Y., Reiss, T., Guiblin, N., Gemeiner, P., Dkhil, B., C. Infante, I.: Size effect on optical and photocatalytic properties in BiFeO₃ nanoparticles, *J. Phys. Chem. C.*, **120**, 3595 – 3601, (2016).

6   Li, S., Lin, Y.H., Zhang, B.P., Wang, Y., Nan, C.W.: Controlled fabrication of BiFeO₃ uniform microcrystals and their magnetic and photocatalytic behaviors, *J. Phys. Chem. C.*, **114**, 2903 – 2908, (2010).

7   Li, Z., Shen, Y., Yang, C., Lei, Y., Guan, Y., Lin, P.Y.H., Liu, D., Nan, C.: Significant enhancement in the visible light photocatalytic properties of BiFeO₃-graphene nanohybrids, *J. Mater. Chem. A.*, 823 – 829, (2013).

8   Bao, X.-M., Cui, J.-F., Sun, H.-X., Liang, W.-D., Zhu, Z.-Q., An, J., Yang, B.-P., La, P.-Q., Li, A.: Facile preparation of superhydrophobic surfaces based on metal oxide nanoparticles, *Appl. Surf. Sci.*, **303**, 473 – 480, (2014).

9   Pahari, D., Das, N.S., Das, B., Chattopadhyay, K.K., Banerjee, D.: Tailoring the optical and hydrophobic property of zinc oxide nanorod by coating with amorphous graphene, *Phys. E Low-dimensional Syst. Nanostructures*, **83**, 47 – 55, (2016).

10   Dave, V., Gupta, H.O., Chandra, R.: Nanostructured hydrophobic DC sputtered inorganic oxide coating for outdoor glass insulators, *Appl. Surf. Sci.*, **295**, 231 – 239, (2014).

11   Lin, S.-S., Liao, C.-S.: The hydrophobicity and optical properties of the HfO₂-deposited glass, *Ceram. Int.*, **39**, 353 – 358, (2013).

12   Azimi, G., Dhiman, R., Kwon, H.M., Paxson, A.T., Varanasi, K.K.: Hydrophobicity of rare-earth oxide ceramics, *Nat. Mater.*, **12**, 315 – 320, (2013).

13   Martínez-González, R., Estelrich, J., Busquets, M.A.: Liposomes loaded with hydrophobic iron oxide nanoparticles: suitable T2 contrast agents for MRI, *Int. J. Mol. Sci.*, **17**, 1209, (2016).

14   Cao, L., Lu, X., Pu, F., Yin, X., Xia, Y., Huang, W., Li, Z.: Facile fabrication of superhydrophobic Bi/Bi₂O₃ surfaces with hierarchical micro-nanostructures by electroless deposition or electrodeposition, *Appl. Surf. Sci.*, **288**, 558 – 563, (2014).

15   Martin, L.W., Chu, Y.-H., Ramesh, R.: Advances in the growth and characterization of magnetic, ferroelectric, and multiferroic oxide thin films, *Mater. Sci. Eng. R Reports*, **68**, 89 – 133, (2010).

16   Baqiah, H., Ibrahim, N.B., Halim, S.A., Flaifel, M.H., Abdi, M.H.: The role of cobalt doping on magnetic and optical properties of indium oxide nanostructured thin film prepared by sol-gel method, *Mater. Res. Bull.*, **63**, 147 – 154, (2015).

17   Baqiah., H., Ibrahim., N.B., Abdi., M.H., Halim., S.A.: Electrical transport, microstructure and optical properties of Cr-doped In₂O₃ thin film prepared by sol-gel method, *J. Alloy. Compd.*, **575**, 198 – 206, (2013).

18   Dong, G., Tan, G., Liu, W., Xia, A., Ren, H.: Effect of tb doping on structural and electrical properties of BiFeO₃ thin films prepared by Sol-Gel technique, *J. Mater. Sci. Technol.*, **30**, 365 – 370, (2014).

19   Hong, D., Yu, S., Cheng, J.: Sm-Ti co-substituted BiFeO₃ thin films prepared by sol-gel technique, *Curr. Appl. Phys.*, **11**, S255 – S259, (2011).

20   Sharma, S., Saravanan, P., Pandey, O.P., Vinod, V.T.P., Černík, M., Sharma, P.: Magnetic behaviour of sol-gel driven BiFeO₃ thin films with different grain size distribution, *J. Magn. Magn. Mater.*, **401**, 180 – 187, (2016).

21   Shirahata, Y., Oku, T.: Characterization and photovoltaic properties of BiFeO₃ thin films, *Coatings,* **6**, 68, (2016).

22   Soram, B.S., Ngangom, B.S., Sharma, H.B.: Effect of annealing temperatures on the structural and optical properties of sol-gel processed nanocrystalline BiFeO₃ thin films, *Thin Solid Films,* **524**, 57 – 61, (2012).

23   Ibrahim, N.B., Al-Shomar, S.M., Ahmad, S.H.: Effect of aging time on the optical, structural and photoluminescence properties of nanocrystalline ZnO films prepared by a sol-gel method, *Appl. Surf. Sci.*, **283**, 599 – 602, (2013).

24   Fu, Q., Cao, C.-B., Zhu, H.-S.: Preparation of alumina films from a new sol-gel route. *Thin Solid Films,* **348**, 99 – 102, (1999).

25   Go, R., López, R., Gómez, R.: Band-gap energy estimation from diffuse reflectance measurements on sol – gel and commercial TiO₂: A comparative study, *J. Sol-Gel Sci. Technol.*, **61**, 1 – 7, (2012).

26   Hauser, A.J., Zhang, J., Mier, L., Ricciardo, R.A., Woodward, P.M., Gustafson, T.L., Brillson, L.J., Yang, F.Y.: Characterization of electronic structure and defect states of thin epitaxial BiFeO₃ films by UV-visible absorption and cathodoluminescence spectroscopies, *Appl. Phys. Lett.*, **92**, 222901 (2008).

27   Chen, X., Zhang, H., Wang, T., Wang, F., Shi, W.: Optical and photoluminescence properties of BiFeO₃ thin films grown on ITO-coated glass substrates by chemical solution deposition, *Phys. status solidi.*, **209**, 1456 – 1460, (2012).

28   Xu, J.-P., Zhang, R.-J., Chen, Z.-H., Wang, Z.-Y., Zhang, F., Yu, X., Jiang, A.-Q., Zheng, Y.-X., Wang, S.-Y., Chen, L.-Y.: Optical properties of epitaxial BiFeO₃ thin film grown on SrRuO₃-buffered SrTiO₃ substrate, *Nanoscale Res. Lett.*, **9**, 188, (2014).

29   Liu, H.L., Lin, M.K., Cai, Y.R., Tung, C.K., Chu, Y.H.: Strain modulated optical properties in BiFeO₃ thin films, *Appl. Phys. Lett.*, **103**, 181907, (2013).

30   Mishra, D.K., Qi, X.: Energy levels and photoluminescence properties of nickel-doped bismuth ferrite, *J. Alloy. Compd.*, **504**, 27 – 31, (2010).

31   Singh, A., Khan, Z.R., Vilarinho, P.M., Gupta, V., Katiyar, R.S.: Influence of thickness on optical and structural properties of BiFeO₃ thin films: PLD grown, *Mater. Res. Bull.*, **49**, 531 – 536 (2014).

32   Ramachandran, B., Dixit, A., Naik, R., Lawes, G., Rao, M.S.R.: Charge transfer and electronic transitions in polycrystalline BiFeO₃, *Phys. Rev. B.*, **82**, 012102, (2010).